the FEBS Journal

# C-terminal, endoplasmic reticulum-lumenal domain of prosurfactant protein C – structural features and membrane interactions

Cristina Casals[1], Hanna Johansson[2], Alejandra Saenz[1], Magnus Gustafsson[2,3], Carlos Alfonso[4], Kerstin Nordling[2] and Jan Johansson[2]

1 Department of Biochemistry and Molecular Biology I & CIBER Enfermedades Respiratorias, Complutense University of Madrid, Spain
2 Department of Anatomy, Physiology and Biochemistry, Swedish University of Agricultural Sciences, The Biomedical Centre, Uppsala, Sweden
3 Department of Medical Biochemistry and Biophysics, Karolinska Institutet, Stockholm, Sweden
4 Centro de Investigaciones Biológicas, Consejo Superior de Investigaciones Científicas, Madrid, Spain

**Keywords**
amyloid disease; Brichos domain; membrane protein; protein–lipid interactions

**Correspondence**
J. Johansson, Department of Anatomy, Physiology and Biochemistry, Swedish University of Agricultural Sciences, The Biomedical Centre, 751 23 Uppsala, Sweden
Fax: +46 18 550762
Tel: +46 18 4714065
E-mail: jan.johansson@afb.slu.se

(Received 27 August 2007, revised 6 November 2007, accepted 4 December 2007)

doi:10.1111/j.1742-4658.2007.06220.x

Surfactant protein C (SP-C) constitutes the transmembrane part of prosurfactant protein C (proSP-C) and is α-helical in its native state. The C-terminal part of proSP-C (CTC) is localized in the endoplasmic reticulum lumen and binds to misfolded (β-strand) SP-C, thereby preventing its aggregation and amyloid fibril formation. In this study, we investigated the structure of recombinant human CTC and the effects of CTC–membrane interaction on protein structure. CTC forms noncovalent trimers and supratrimeric oligomers. It contains two intrachain disulfide bridges, and its secondary structure is significantly affected by urea or heat only after disulfide reduction. The postulated Brichos domain of CTC, with homologs found in proteins associated with amyloid and proliferative disease, is up to 1000-fold more protected from limited proteolysis than the rest of CTC. The protein exposes hydrophobic surfaces, as determined by CTC binding to the environment-sensitive fluorescent probe 1,1′-bis(4-anilino-5,5′-naphthalenesulfonate). Fluorescence energy transfer experiments further reveal close proximity between bound 1,1′-bis(4-anilino-5,5′-naphthalenesulfonate) and tyrosine residues in CTC, some of which are conserved in all Brichos domains. CTC binds to unilamellar phospholipid vesicles with low micromolar dissociation constants, and differential scanning calorimetry and CD analyses indicate that membrane-bound CTC is less structurally ordered than the unbound protein. The exposed hydrophobic surfaces and the structural disordering that result from interactions with phospholipid membranes suggest a mechanism whereby CTC binds to misfolded SP-C in the endoplasmic reticulum membrane.

Amyloid diseases represent a growing medical problem in which specific proteins are converted from their soluble native structure and form insoluble fibrils. The fibrils are composed of a cross-β-sheet structure, in which the strands are oriented perpendicular to the fibril axis [1]. The amyloid diseases include Alzheimer's

**Abbreviations**
bis-ANS, 1,1′-bis(4-anilino-5,5′-naphthalenesulfonate); CTC, C-terminal domain of prosurfactant protein C; DPPC, 1,2-dipalmitoyl-phosphatidylcholine; DSC, differential scanning calorimetry; ER, endoplasmic reticulum; FRET, fluorescence resonance energy transfer; ILD, interstitial lung disease; LUV, large unilamellar vesicles; POPC, 1-palmitoyl-2-oleoyl-phosphatidylcholine; POPE, 1-palmitoyl-2-oleoyl-phosphatidylethanolamine; POPG, 1-palmitoyl-2-oleoyl-phosphatidylglycerol; $T_m$, gel-to-fluid phase transition temperature.

disease, the spongiform encephalopathies or prion diseases, and type II diabetes mellitus. Knowledge of the pathophysiological mechanisms in amyloid diseases is incomplete, but they probably include cytotoxicity elicited by the amyloid deposits as such and/or by soluble intermediates on the pathway from the native to the fibrillar state [2].

Lung surfactant protein C (SP-C) is a 35-residue transmembrane α-helical lipopeptide that is exclusively produced by alveolar type II cells. SP-C is secreted into the alveolar space in order to promote spreading and stability of phospholipids at the alveolar air–liquid interface [3,4]. The α-helical structure of SP-C is metastable, due to a poly-Val sequence, and spontaneously converts to β-sheet aggregates and amyloid fibrils [5]. This property of SP-C appears to be relevant to human disease. The fibrillar form of SP-C has been isolated from lung lavage fluid obtained from patients suffering from pulmonary alveolar proteinosis [6]. Moreover, recently discovered mutations in the SP-C precursor [prosurfactant protein C (proSP-C)] are associated with interstitial lung disease (ILD), misfolding of proSP-C in the endoplasmic reticulum (ER), cellular toxicity, and reduced levels of mature SP-C in the alveoli [7–11]. proSP-C is a 197-residue transmembrane protein with a type II orientation in the ER membrane; that is, the N-terminus is localized on the cytosolic side. Mature SP-C corresponds to residues 24–58. Residues 1–23 of proSP-C constitute an N-terminal propart, and residues 59–197 constitute a C-terminal propart localized in the ER lumen [see Fig. 3 below for the amino acid sequence of the C-terminal part of proSP-C (CTC)].

CTC contains a ~ 100-residue Brichos domain, covering the region from residue 94 to the C-terminal end. The name Brichos refers to the fact that the domain was initially found in proteins belonging to the Bri family, associated with familial British and Danish dementia, in chondromodulin, associated with chondrosarcoma, and in proSP-C [12]. These proteins are all made as transmembrane precursors that are processed into fragments by proteolysis. Recently, the Brichos domain has been found also in other proteins, including a protein (TFIZ1) that binds trefoil domains [13]. The Brichos domain may be involved in folding and processing of the precursors and in binding to other polypeptides [12,14]. The structural properties have not been experimentally investigated for any Brichos domain, and it lacks clearly homologous proteins, although it has been compared to the apical domain of the chaperone GroEL [12].

We have recently found that: (a) expression of proSP-$C^{L188Q}$, a mutant associated with ILD, in cell culture, results in formation of intracellular amyloid-like aggregates; (b) replacement of the metastable poly-Val part with a thermodynamically stable poly-Leu part [15] stabilizes proSP-$C^{L188Q}$; (c) transfection with CTC stabilizes proSP-$C^{L188Q}$; (d) recombinant wild-type CTC, but not $CTC^{L188Q}$, binds to SP-C that is in the β-strand conformation; and (e) CTC added *in trans* prevents SP-C from forming amyloid fibrils [14]. These findings suggest that CTC works as a specific scavenger of misfolded SP-C in the ER and thereby prevents aggregation and amyloid fibril formation. With the aim of defining how CTC can scavenge misfolded, membrane-bound SP-C, we have now investigated its structure, domain organization, stability, and phospholipid interactions.

## Results

### Quaternary structure

#### Analytical ultracentrifugation

Sedimentation velocity was used to estimate the association state of the protein and its degree of size polydispersity. Figure 1A shows the sedimentation coefficient distribution of CTC, which reveals that the protein is heterogeneous in size. The main sedimenting species (~ 85% of the loading concentration) has an *s*-value of 3.1 ± 0.2 S, and two minor species (~ 5% each) have *s*-values of 1.9 and 5 S, respectively. These results agree well with the distribution of species found by electrophoresis under native conditions (Fig. 1B). In order to determine the mass of the main species observed, parallel sedimentation equilibrium experiments were performed. Figure 1C shows the protein gradient at sedimentation equilibrium. The best fit analysis, assuming a single sedimenting species, yielded an average molecular mass of 52 000 ± 2000 Da, which is compatible with the size expected for a CTC trimer (54 800 Da). The derived mass was essentially invariant over protein concentrations from 0.05 to 0.45 $mg{\cdot}mL^{-1}$. The hydrodynamic behavior of the protein, taking into account the sedimentation velocity and equilibrium data, deviates slightly from that expected for a globular trimer (frictional ratio $f/f_o = 1.6$).

#### MS

ESI MS of CTC in aqueous buffer, pH 6.9, shows mainly trimers, but dimers of trimers, trimers of trimers and tetramers of trimers (i.e. hexamers, nonamers and dodecamers) are also clearly visible (Fig. 2). Weak signals corresponding to monomers, dimers, tetramers, pentamers, heptamers and possibly octamers exist

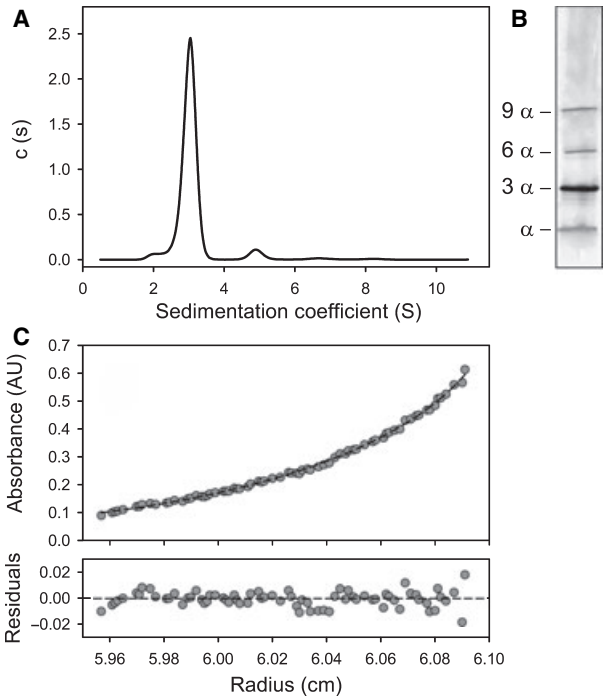


**Fig. 1.** Oligomerization state of CTC. (A) Sedimentation coefficient distribution of 0.45 mg·mL$^{-1}$ CTC at 20 °C. (B) Native PAGE of CTC. The labels on the left indicate bands that are compatible with monomers (α), trimers (3α), hexamers (6α), and nonamers (9α), according to sedimentation velocity and equilibrium data (A, C) and MS data (Fig. 2). (C) Sedimentation equilibrium data (gray dots) and the best fit analysis (solid line), assuming a single sedimenting species. The lower panel shows residuals between estimated values and experimental data for one-component fit.

(data not shown). The largest oligomer uniquely identified was a dodecamer, representing a molecular mass of 219 kDa. For trimers, a complete charge state envelope between 11 and 26 charges (*m/z* 4982–2108) was observed, and for hexamers and nonamers, complete envelopes between 20 and 35 charges (*m/z* 5480–3132) and between 28 and 37 charges (*m/z* 5872–4444), respectively, were observed. An incomplete charge state envelope between 48 and 66 charges (*m/z* 4567–3322) was observed for dodecamers. Also, a complete charge state envelope between 8 and 16 charges (*m/z* 2284–1143) was observed for monomers, but its strongest peak constituted only 0.6% of the intensity of the peak at *m/z* 3654, which mainly corresponds to a trimer with 15 charges (Fig. 2).

For mass determination of the denatured CTC monomer, a complete charge state envelope between 10 to 18 charges was used for iterative deconvolution onto a true mass scale, giving an average molecular mass of 18 263.71 Da. The theoretical average mass of the protein is 18 264.89 Da with all four Cys residues oxidized (see below), which is in agreement with the experimental result, giving a mass accuracy of 65 p.p.m.

## Structure, stability and hydrophobic surface

### Disulfide bridges

CTC contains four Cys residues. The mass of CTC monomers determined by MALDI MS (18 264.1 Da; supplementary Fig. S1A), like the mass of denatured CTC determined by ESI MS (see above), was indeed in almost exact agreement with its calculated mass, provided that all four Cys residues are engaged in disulfide bridges (18 264.9 Da). This shows that CTC contains two intramolecular disulfides. For determination of half-cystine linkages, trypsin cleavage and identification of liberated peptides by MALDI MS was used. This showed two fragment ions that both correspond to three peptides linked via two disulfide bridges. The $[M + H]^+$ ion at 9272.0 corresponds to peptides covering residues 82–125, 141–153, and 168–197, whereas the $[M + H]^+$ ion at 9400.4 corresponds to peptides 82–125, 140–153, and 168–197 (supplementary Fig. S1B; see Fig. 3 for the amino acid sequence of CTC). These fragments show that one of the two juxtaposed Cys residues at positions 120 and 121 forms a disulfide with Cys148 and the other forms a disulfide with Cys189. The juxtaposition of Cys120 and Cys121 makes it difficult to cleave the polypeptide chain in between these residues, in order to unambiguously assign their disulfide partners. Cys121 and Cys189 are strictly conserved in all Brichos domains described so far, whereas Cys120 and Cys148 lack counterparts in other Brichos domains and are not conserved in all proSP-C sequences [12]. These data strongly suggest that the disulfide pairings in CTC are Cys120–Cys148 and Cys121–Cys189 (Fig. 3).

### Limited proteolysis

CTC was treated with trypsin at a molar ratio of ~ 1300 : 1 and at room temperature. Analysis of the cleavage kinetics by MALDI MS showed that the sensitivity towards trypsin differed > 1000-fold between the possible cleavage sites (Fig. 3). Cleavages after Lys63 and Arg81 occurred first and were observed after 25 s. Cleavages after Lys160 and Arg167 were observed after 6 min. The most resistant cleavage sites were those that follow Lys125 (cleavage first observed after 2 h), Arg139 (cleavage observed after 4 h), and Lys140 (cleavage after 8 days). Cleavages after Lys114 and Lys153 were observed first after 8 days and 19 h, respectively. This resistance to cleavage, however, can be explained by the presence of Pro at positions 115

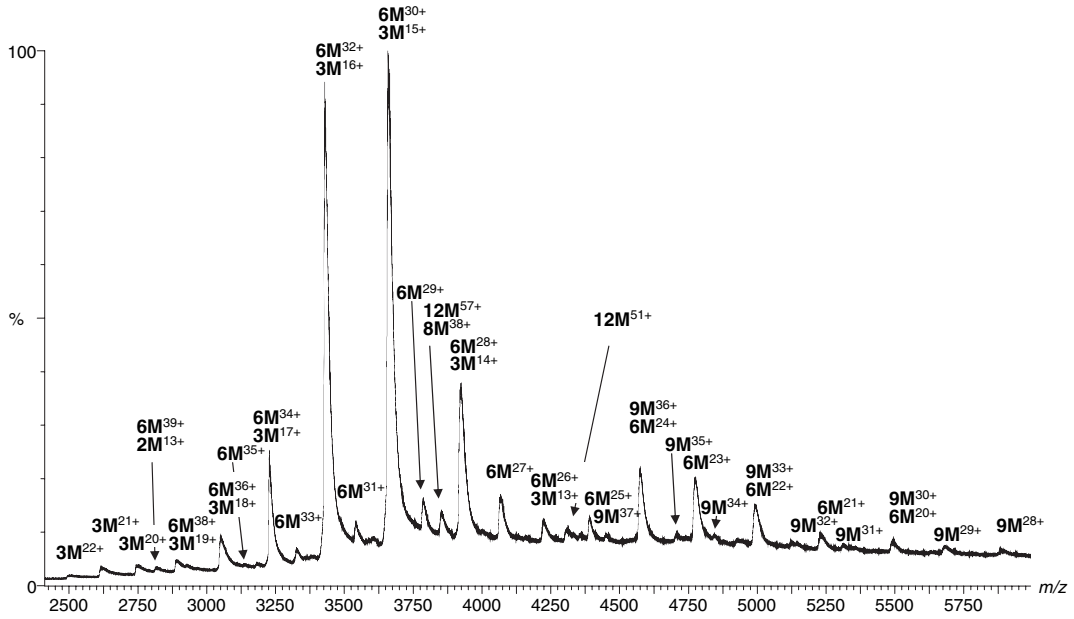


**Fig. 2.** ESI mass spectrum of CTC. Ions are labeled with their most likely oligomeric state and number of charges. Complete charge state envelopes are labeled for a possible trimer, hexamer, and monomer. A complete envelope was not detected for a possible dodecamer, but ions that could be unambiguously assigned (e.g. $12M^{51+}$) are indicated.

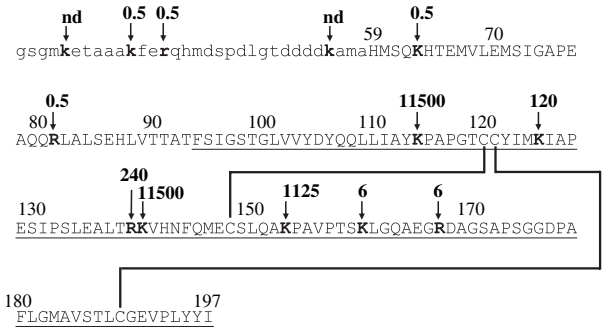


**Fig. 3.** Limited proteolysis of CTC. The amino acid sequence of human CTC is in upper-case letters, and the sequence of the S-tag is in lower-case letters. The numbering refers to the positions in the full-length proSP-C sequence. The postulated Brichos domain is underlined. The arrows mark trypsin cleavage sites and the time in minutes after which the cleavages were first observed. The lines connecting Cys residues represent the disulfide pairings now identified. nd, cleavage not detected.

and 154. The pattern that emerges from these experiments is that the CTC Brichos domain is much more resistant to cleavage than the preceding part.

### Urea-induced and temperature-induced unfolding

CD spectra of nonreduced and reduced CTC in the presence of increasing amounts of urea are shown in Fig. 4A,B. Nonreduced CTC showed small and continuous changes in the spectra between 0 and 8 M urea, whereas for reduced CTC, major changes took place between 4 and 7 M urea. The residual molar ellipticity at 222 nm versus urea concentration (Fig. 4C) showed cooperative behavior, with a midpoint at 5.5 M urea for reduced CTC, whereas no cooperative unfolding was seen without reduction.

Similar results as observed in the urea experiments were obtained by heating from 20 °C to 90 °C. Nonreduced CTC only showed a small linear decrease in ellipticity at 222 nm above ~ 60 °C, whereas reduced CTC gave a sharp transition with a midpoint at about 68 °C (supplementary Fig. S2).

### Interaction with 1,1′-bis(4-anilino-5,5′-naphthalenesulfonate) (bis-ANS)

The fluorescence intensity and emission maximum wavelength ($\lambda_{max}$) of bis-ANS depend on its environment, and are commonly used to probe accessible hydrophobic surfaces of proteins. The fluorescence intensity of bis-ANS increased > 7-fold and its $\lambda_{max}$ was blue-shifted from 525 to 482 nm upon binding to CTC (supplementary Fig. S3). The magnitude of the fluorescence change increased as a function of CTC concentration and was saturable. The apparent equilibrium dissociation constant ($K_d$) for CTC–bis-ANS complexes was 1.7 ± 0.3 μM ($n$ = 2), assuming a molecular mass of 18.2 kDa for monomeric CTC.

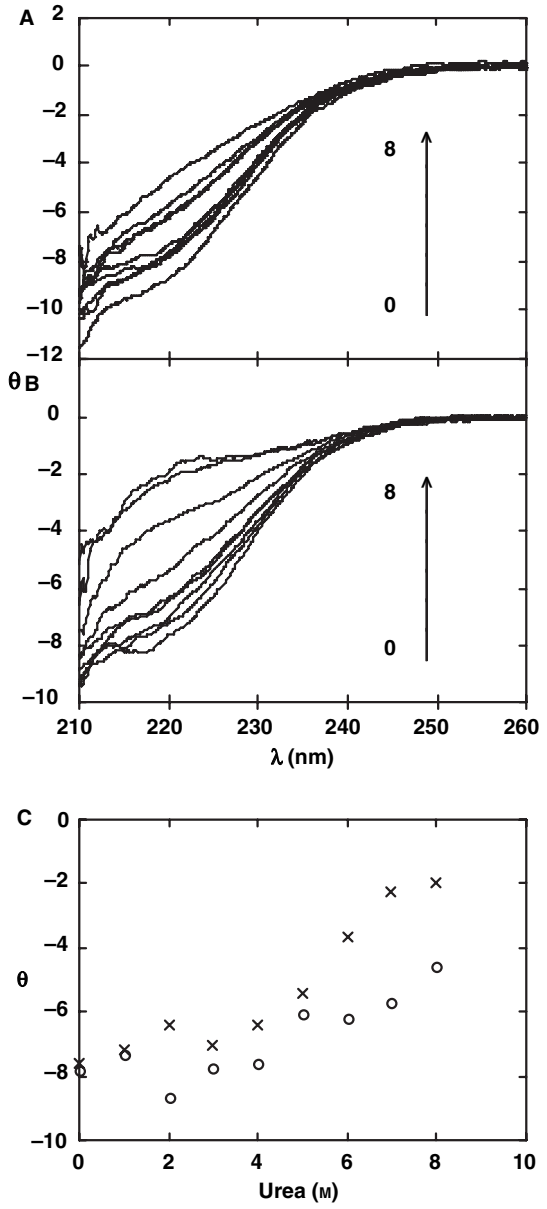


**Fig. 4.** Effects of urea on CTC secondary structure. CD spectra of CTC in 0–8 M urea increasing by 1 M steps, as indicated by the arrows. (A) Nonreduced CTC. (B) Reduced CTC. (C) Residual molar ellipticity at 222 nm of reduced (crosses) and nonreduced (open circles) CTC versus urea concentration. The residual molar ellipticity (θ) is expressed in kdeg·cm$^{-2}$·dmol$^{-1}$.

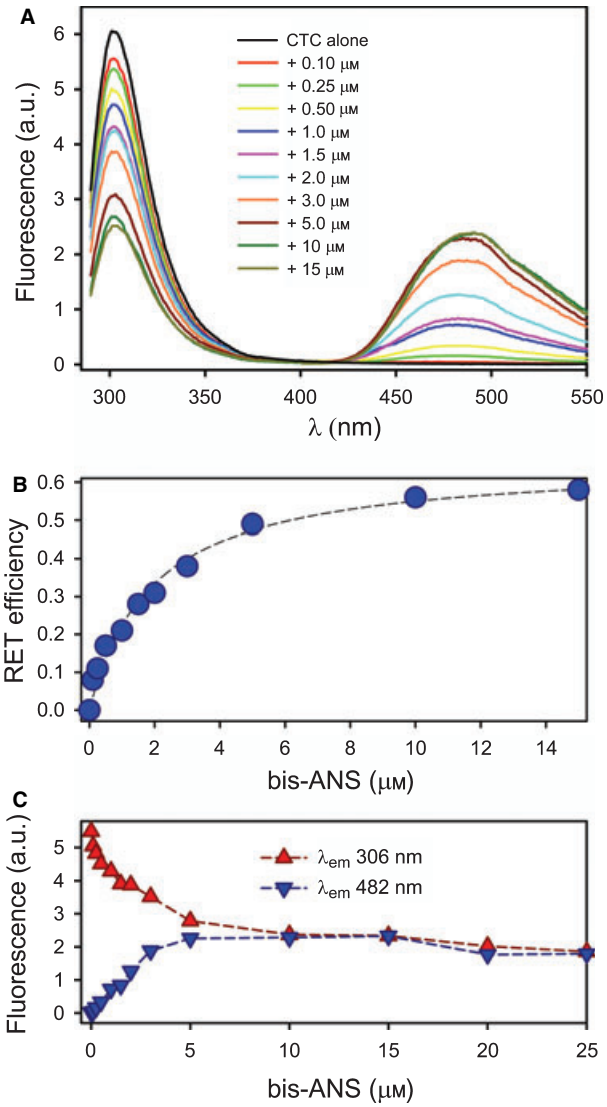


**Fig. 5.** Energy transfer between Tyr and bound bis-ANS in CTC. (A) Fluorescence emission spectra of CTC in the absence (black line) and presence of increasing concentrations of bis-ANS. (B) The efficiency of energy transfer from Tyr to bis-ANS. (C) Data from the spectra shown in (A) were used to construct a plot of the relative fluorescence intensity at 306 nm (blue circles, representing Tyr fluorescence) and the relative fluorescence at 482 nm (red circles, representing bound bis-ANS fluorescence) versus bis-ANS concentration.

CTC contains six Tyr residues and no Trp residues. To determine whether Tyr residues are close to the bis-ANS-binding site in CTC, fluorescence resonance energy transfer (FRET) studies were performed. Figure 5A shows the emission spectra of CTC after excitation at 280 nm in the presence of different concentrations of bis-ANS. Upon addition of increasing bis-ANS concentrations, there was a gradual decrease in Tyr fluorescence at 306 nm, concurrent with an increase in the bis-ANS fluorescence at 482 nm. As free bis-ANS does not emit when excited at 280 nm, the increase in fluorescence at 482 nm indicates energy transfer from CTC Tyr residues to bis-ANS bound to surface-exposed hydrophobic sites. FRET data were also used to determine the affinity of bis-ANS for

CTC. The $K_d$ calculated from energy transfer efficiency from Tyr residues to bis-ANS was 1.8 ± 0.2 μM (Fig. 5B,C), similar to that calculated from bis-ANS fluorescence titration experiments (supplementary Fig. S3). Considering the dependence of energy transfer efficiency on distance between donor and acceptor, FRET experiments indicate molecular proximity of Tyr residues in CTC and the bound bis-ANS.

## Interaction with phospholipid vesicles

### Intrinsic fluorescence experiments

The intrinsic Tyr fluorescence of CTC was measured upon titration with large unilamellar vesicles (LUVs) composed of 1-palmitoyl-2-oleoyl-phosphatidylcholine (POPC), 1-palmitoyl-2-oleoyl-phosphatidylglycerol (POPG), POPC/POPG (1 : 1, w/w), and POPC/1-palmitoyl-2-oleoyl-phosphatidylethanolamine (POPE) (1 : 1, w/w). As shown in Fig. 6A, increasing concentrations of LUVs progressively reduced the fluorescence emission intensity, reaching saturation at a phospholipid/protein weight ratio of 10 : 1. For all LUVs, a sharp decrease in fluorescence intensity at 305 nm was observed, reaching saturation at a phospholipid concentration of 0.1 mM (CTC subunit concentration was 1 μM, Fig. 6B). Estimated $K_d$ values for CTC–phospholipid complexes were in the low micromolar range (Fig. 6B).

### Effect of phospholipid vesicles on CTC secondary structure

The CD spectrum of CTC in the absence of lipids (Fig. 7, black line) indicates 32% α-helix, 34% β-sheet, and about 20% random coil structures (Table 1). The binding of CTC to increasing concentrations of LUVs progressively altered the CD signal. The negative ellipticity increased and the minimum was blue-shifted (Fig. 7). For all types of phospholipid vesicles, the percentages of α-helix and β-sheet structures decreased, whereas that of random coil structure increased (Table 1). This effect was most prominent with POPC and 1,2-dipalmitoyl-phosphatidylcholine (DPPC) vesicles.

### Effect of phospholipid vesicles on CTC thermal unfolding

Thermal unfolding of nonreduced CTC was not observed by CD (supplementary Fig. S2). Therefore, differential scanning calorimetry (DSC) was used to determine the thermal stability of free and membrane-bound CTC. The melting curve displayed one heat absorption peak over a temperature range of 20–95 °C (Fig. 8A, scan 1). The apparent $T_m$ value was 66.4 ± 0.4 °C ($n$ = 5). Thermal unfolding of CTC was not completely reversible; after a cycle of heating and cooling, there was a distortion with the appearance of a low-temperature endotherm (Fig. 8A, scan 2). The heat capacity curves for the second and third scans overlapped. Interestingly, the melting curve of reduced CTC showed a low-temperature endotherm, similar to scan 2 of the nonreduced protein (data not shown).

The melting curves of membrane-bound CTC showed two transitions with maxima at 59 °C and 66–67 °C (Fig. 8B). The first, second and third heat capacity curves of membrane-bound CTC overlapped.

## Discussion

The present study shows that human CTC is oligomeric, exposes hydrophobic surfaces, and binds to phospholipid membranes with concomitant structural disordering of the protein. CTC mainly forms trimers, but also some larger oligomers (Fig. 1). Analytical ultracentrifugation lacks the ability to exactly determine the molecular mass, and the composition of the

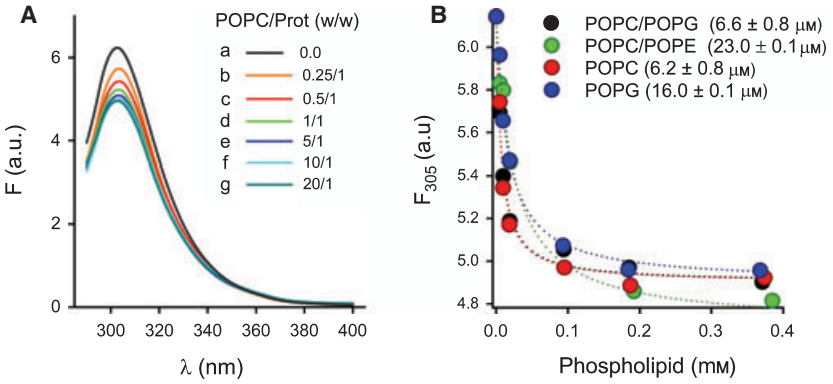


**Fig. 6.** CTC binds to phospholipid vesicles. (A) Fluorescence emission spectra of CTC in the absence and presence of different amounts of POPC vesicles at 25 °C. The phospholipid/CTC weight ratios are indicated. (B) Net change in fluorescence emission intensity at 305 nm versus phospholipid concentration. Estimated $K_d$ values for CTC–phospholipid vesicle complexes are given in parentheses.

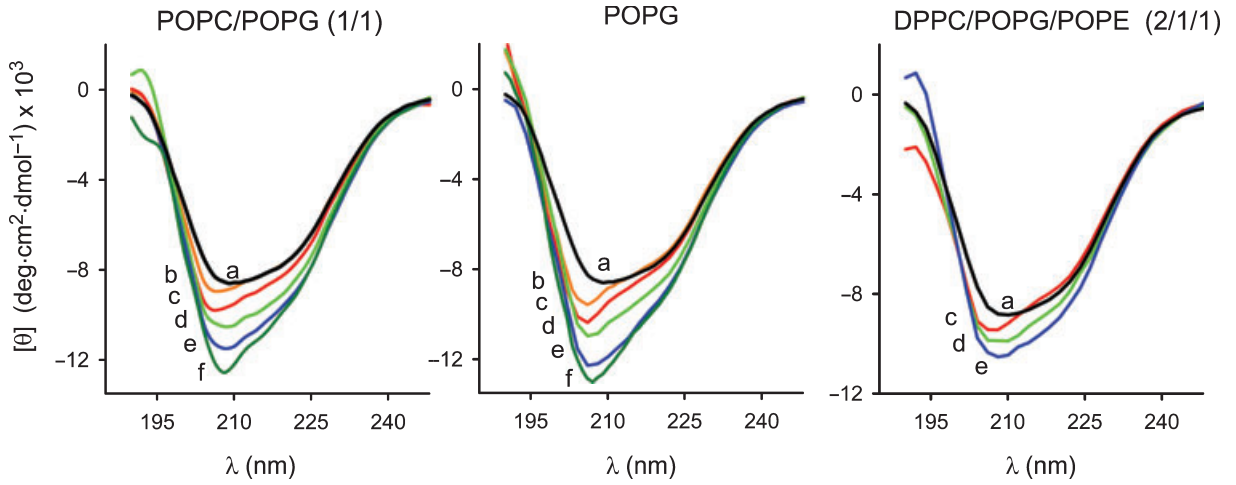


**Fig. 7.** Effect of phospholipid vesicles on CTC secondary structure. The composition of the phospholipid vesicles is given above each set of spectra. The total phospholipid/CTC weight ratios were: no phospholipid (A); 0.25 : 1 (B); 1 : 1 (C); 5 : 1 (D); 10 : 1 (E); and 20 : 1 (F).

**Table 1.** Secondary structure contents of CTC in the absence and presence of phospholipid vesicles. The phospholipid/protein weight ratio was 10 : 1.

| | % Secondary structure | | | |
|---|---|---|---|---|
| | α-Helix | β-Sheet | β-Turn | Random |
| CTC | 32 | 34 | 15 | 19 |
| + POPC | 26 | 20 | 15 | 39 |
| + DPPC | 26 | 22 | 12 | 39 |
| + POPG | 27 | 24 | 15 | 33 |
| + POPC/POPG (1 : 1, w/w) | 27 | 23 | 14 | 36 |
| + DPPC/POPG (1 : 1, w/w) | 27 | 24 | 12 | 34 |
| + POPC/POPE (1 : 1, w/w) | 26 | 28 | 11 | 34 |
| + DPPC/POPG/POPE (2 : 1 : 1, w/w) | 28 | 27 | 12 | 34 |

larger complexes was therefore difficult to assign. ESI MS can be used to study protein interactions in the gas phase under pseudo-physiological conditions [16,17]. The ESI data show that CTC forms trimers and oligomers of trimers (Fig. 2). Chemical crosslinking experiments have shown that proSP-C in cell culture forms dimers and larger oligomers. Also, proSP-C(24–58), i.e. the mature SP-C part, was crosslinked into mainly dimers but also larger oligomers, indicating that proSP-C oligomerization in the ER membrane is mediated by the SP-C part [18]. Our data show that CTC forms trimers in the absence of the remaining parts of proSP-C, which suggests that the C-terminal part can also contribute to proSP-C oligomerization. ILD-associated mutations in the Brichos domain of proSP-C are present on one allele only, but still cause near complete absence of mature SP-C [4]. The ability of CTC to oligomerize may partly explain this dominant negative effect, if mutant and wild-type proSP-C form co-oligomers that are trapped in the ER.

The Brichos domain was postulated from multiple sequence alignments [12]. Limited proteolysis of CTC (Fig. 3) gives experimental support for the existence of a folded entity that agrees well with the proposed

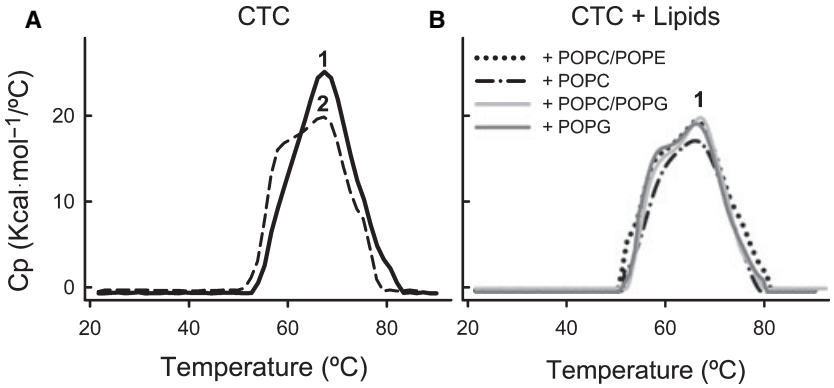


**Fig. 8.** Thermal unfolding of CTC in the absence and presence of phospholipid vesicles. The temperature dependence of specific heat capacity at constant pressure, $C_p$, in the absence (A) and presence (B) of different phospholipid vesicles. The phospholipid/protein weight ratio was 10 : 1.

boundaries of the Brichos domain. The region between residues 160 and 170 appears to be less protected from proteolysis than the rest of CTC. It is notable that this region is localized in a part of proSP-C where residue exchanges between species are frequent as compared to most of proSP-C (see http://www.pdg.cnb.uam.es/BRICHOS for alignment of proSP-C sequences), and that *Xenopus laevis* proSP-C [19] has a deletion in this region. The non-Brichos part of CTC is readily cleaved by trypsin, which indicates that it is structurally flexible. Interestingly, this segment is evolutionarily well conserved, and ILD-associated mutations herein, e.g. the common proSP-$C^{I73T}$, appear to give rise to a different phenotype than mutations in the Brichos domain [4].

CTC exposes hydrophobic surfaces with contributions from Tyr residues (Fig. 5). It is tempting to speculate that the side chains of some of the six Tyr residues in CTC (Fig. 3) might form an apolar pocket involved in the recognition of poly-Val peptides and lipid-bound nonhelical SP-C [14]. The Tyr residues are well conserved in proSP-C, and the mutation proSP-$C^{Y104H}$ is linked to ILD [20]. Furthermore, Tyr residues at positions 106, 122 and 195 of proSP-C are highly conserved (or replaced by Phe) in all Brichos domains [12].

CTC binds to both zwitterionic and anionic phospholipid vesicles (Fig. 6). The slightly lower $K_d$ for CTC binding to POPC than for binding to POPG indicates a somewhat higher affinity for the phosphocholine headgroup. However, when POPC was mixed with POPE, but not with POPG, the binding affinity decreased slightly. With respect to the physical state of the phospholipid vesicles, CTC binds equally to saturated (DPPC) and unsaturated (POPC) vesicles (data not shown). The low micromolar $K_d$ values for CTC–phospholipid vesicles indicate high binding affinities, comparable to those determined for tightly associated membrane proteins such as spectrin ($K_{d\ PC} = 0.5$ μM) [21], cecropin P1 ($K_{d\ PC/PS} = 8$ μM) [22], or cytochrome *c* oxidase ($K_{d\ PC/PG} = 26$ μM) [23]. This suggests that the C-terminal domain of proSP-C will also associate with phospholipid membranes after it has been proteolytically released from proSP-C.

CD spectroscopy shows that CTC contains a mixed secondary structure and that the disulfides are essential for stability (Fig. 4, Table 1). Thermal unfolding of CTC measured with DSC shows a broad endotherm (Fig. 8), which indicates that the structure unfolds gradually, rather than in a cooperative manner. It is plausible that the oligomeric nature contributes to this behavior. CTC binding to phospholipid vesicles resulted in the appearance of a reversible low-temperature endotherm (Fig. 8). This is consistent with a phospholipid-induced increase in random structure and a decrease in ordered structures seen by CD spectroscopy (Fig. 7, Table 1). Collectively, the results from DSC and CD experiments indicate that membrane-bound CTC is structurally less ordered than the free protein. Structural disordering of CTC upon membrane binding is intriguing, as a less ordered structure will be more adaptable in binding to misfolded SP-C. The structural properties of CTC, in particular exposed hydrophobic surface and membrane interactions, are thus compatible with a role as a scavenger of misfolded SP-C in the ER membrane. Disulfide bridges and Tyr residues are here shown to be important for CTC stability and exposure of hydrophobic surface, respectively. Cys and Tyr residues are particularly well conserved in the Brichos domain [12], which suggests that some of the features of CTC now described are applicable to other Brichos domains as well.

## Experimental procedures

### Materials

bis-ANS was obtained from Molecular Probes, Inc. (Eugene, OR, USA). Synthetic phospholipids were obtained from Avanti Polar Lipids (Birmingham, AL, USA). Methanol and chloroform used to dissolve lipids were HPLC-grade (Scharlau, Barcelona, Spain). All other reagents were of analytical grade and were obtained from Merck (Darmstadt, Germany).

### Expression and isolation of CTC

CTC was expressed and purified as described previously [14]. In essence, a fragment covering residues 59–197 of human proSP-C was expressed as a fusion protein with thioredoxin-tag, $His_6$-tag and S-tag in *Escherichia coli*. The protein was purified using affinity chromatography and ion exchange chromatography. Thrombin was used to remove the thioredoxin-tag and $His_6$-tag. The protein purity on SDS/PAGE was > 90%. Native PAGE was performed at 4 °C with a 4–20% gradient polyacrylamide gel (Biorad, Hercules, CA, USA) for 16 h. CTC was visualized by silver stain.

### Analytical ultracentrifugation

Sedimentation velocity experiments were performed at 50 000 r.p.m. and 20 °C in a Beckman XL-A ultracentrifuge (Beckman-Coulter Inc., Fullerton, CA, USA) with a UV–visible optics detector, using an An-50Ti rotor and double-sector 12 mm centerpieces of Epon-charcoal. Sedimentation profiles were registered every 5 min at 235, 260

or 280 nm. Typically, 0.45 mg·mL$^{-1}$ CTC in 20 mM phosphate buffer (pH 7.4) were used. The sedimentation coefficient distributions were calculated by least-squares boundary modeling of sedimentation velocity data using the $c(s)$ method [24,25], as implemented in the SEDFIT program, from which the corresponding $s$-values were determined.

Sedimentation equilibrium short-column experiments (70 μL of protein, loading concentrations 0.05, 0.075, 0.1, 0.15, 0.225 and 0.45 mg·mL$^{-1}$ in 20 mM phosphate buffer, pH 7.4) were done at 16 000, 18 000, 20 000 and 35 000 r.p.m. by taking absorbance scans when sedimentation equilibrium was reached. High-speed sedimentation (50 000 r.p.m.) was conducted afterwards for baseline corrections. The buoyant molecular masses of the protein were determined by fitting a sedimentation equilibrium model of a single sedimenting solute to individual data using the programs EQASSOC [26] or HeteroAnalysis [27]. These values were converted to the corresponding average molecular masses by using 0.731 mL·g$^{-1}$ as the partial specific volume of CTC, calculated from the amino acid composition with the program SEDNTERP [28].

## ESI MS

Data were acquired on a QTOF Ultima API mass spectrometer, (Waters, Milford, MA, USA) equipped with a Z-spray source operated in the positive-ion mode. Scans between 800 and 6000 $m/z$ were acquired. Samples were introduced via a nanoflow electrospray interface from metal-coated borosilicate glass capillary needles (Proxeon Biosystems, Odense, Denmark), and the source temperature was 80 °C. The capillary voltage was between 1.2 and 1.9 kV, and cone and RF lens potentials were 100 and 38 V, respectively. The pumping of the ESI interface region was restricted; backing pirani vacuum gauge from 1.8 to 1.95 mbar, and analyzer pressure $5.85 \times 10^{-5}$ mbar. Argon gas was used as collision gas, and the collision voltage was 10 V. The instrument was operated in single reflector mode at a resolution of 10 000 (full width half maximum definition), and the mass scale was calibrated against poly(ethylene glycol)-3400. CTC stock solution (1164 μM in 20 mM sodium phosphate buffer, 30 mM NaCl, pH 7.4) was diluted to 11 μM in 10 mM ammonium acetate buffer (pH 6.9) prior to analysis. A mass spectrum of monomeric CTC denatured in 30% acetonitrile/0.1% acetic acid was deconvoluted onto a true mass scale using the maximum entropy function of the MASSLYNX software package. The processing parameters were as follows: the output mass range was 15 000–21 000 Da at a 'resolution' of 1.0 Da per channel; the damage model was used with the uniform Gaussian parameter set to 1.0 Da width at half-height; the minimum intensity ratios between successive peaks were 10% (left and right). The deconvoluted spectrum was mass centroided using 80% of the peak and a minimum peak width at half-height of two channels.

## MALDI MS

Spectra were acquired on a Bruker Autoflex (Bruker Daltonics, Billerica, MA, USA) operated in linear mode ($m/z$ 1800–26 000) or in reflector mode ($m/z$ 800–5000). In both cases, delayed extraction was employed. When peptides < 4000 Da were analyzed, 0.5 μL of sample was added to a Bruker standard steel target and cocrystallized with 0.5 μL of α-cyano-4-hydroxycinnamic acid (3 mg·mL$^{-1}$) dissolved in 70% acetonitrile/0.1% trifluoroacetic acid. When proteins > 4000 Da were analyzed, 0.5 μL of sample was deposited on top of a thin layer of sinapinic acid precrystallized from a 30 mg·mL$^{-1}$ solution in acetone, and cocrystallized with 0.5 μL of sinapinic acid (30 mg·mL$^{-1}$) dissolved in 50% acetonitrile/0.1% trifluoroacetic acid.

## Limited proteolysis

Two hundred micrograms of CTC and 0.2 μg of modified trypsin (Promega, Madison, WI, USA) were dissolved in 100 μL of 50 mM ammonium bicarbonate buffer (pH 7.8) at room temperature. At different time points, between 25 s and 8 days, 1 μL aliquots were removed and added to 9 μL of ice-cold 30% acetonitrile/0.1% trifluoroacetic acid and kept on ice until analysis by MALDI MS.

## Preparation of phospholipid vesicles

Freshly prepared unilamellar vesicles were used. Phospholipids were dissolved in chloroform/methanol 3 : 1 (v/v), and evaporated under a stream of nitrogen and under reduced pressure overnight. Vesicles were prepared at a total phospholipid concentration of 1 mg·mL$^{-1}$ by hydrating lipid films in 150 mM NaCl, 0.1 mM EDTA, and 5 mM Tris/HCl (pH 7.4), and allowing them to swell for 1 h at a temperature above their $T_m$. After vortexing, the resulting multilamellar vesicles were sonicated at the same temperature in a UP 200S sonifier with a 2 mm microtip. The final lipid concentration was assessed by phosphorus determination. For vesicle-size analysis, quasi-elastic light scattering was used. DPPC/POPG (1 : 1, w/w), POPC/POPG (1 : 1, w/w) and POPG vesicles consisted of a major population (85%) of unilamellar vesicles (mean diameter 95 ± 15 nm) and a minor population (15%) of multilamellar vesicles that was removed by centrifugation. Vesicles of DPPC, POPC and POPC/POPE (1 : 1, w/w) consisted of a major population (60–70%) of unilamellar vesicles (mean diameter 110–160 nm).

## CD spectroscopy

For unfolding experiments, CD spectra in the far-UV region (190–260 nm) were recorded either at 22 °C for CTC

(20 μM) in 20 mM $NaH_2PO_4$ and 5 mM NaCl buffer (pH 7.4), containing from 0 to 8 M urea, or between 20 °C and 90 °C at 222 nm, with increments of 2 °C·min$^{-1}$, for CTC (15 μM) in 10 mM $NaH_2PO_4$ and 50 mM NaCl (pH 7.4). Reduction was achieved by incubation with 300 μM dithiothreitol at 37 °C for 2 h. Spectra were recorded with a Jasco J-810-150S spectropolarimeter (Jasco, Tokyo, Japan), using a bandwidth of 1 nm and a response time of 2 s, and 10 data points per nanometer were collected. Each spectrum is the average of three scans.

Far-UV CD spectra of CTC in the presence of phospholipid vesicles were obtained on a Jasco J-715 spectropolarimeter. Four scans were accumulated and averaged for each spectrum. The acquired spectra were corrected by subtracting the appropriate blank runs (of buffer or phospholipid vesicle solutions), and subjected to noise reduction analysis; data are presented as molar ellipticities (θ) (kdeg·cm$^{-2}$·dmol$^{-1}$), using 130 Da as the average residue mass. All measurements were performed in 5 mM Tris/HCl buffer (pH 7.4), containing 150 mM NaCl at 25 °C. The protein concentration was 10 μM. Estimation of the secondary structure content from the CD spectra was performed after deconvolution of the spectra into four simple components (α-helix, β-sheet, β-turn, and random coil) according to the convex constraint algorithm [29].

### Fluorescence measurements

Fluorescence measurements were carried out using an SLM-Aminco AB-2 spectrofluorimeter with a thermostated cuvette holder (Thermo Spectronic, Waltham, MA, USA) (± 0.1 °C), using 5 × 5 mm path-length quartz cuvettes. Fluorescence emission spectra of CTC (1 μM) with or without phospholipid vesicles or bis-ANS were measured at 25 °C in 5 mM Tris/HCl buffer (pH 7.4) and 150 mM NaCl. Excitation was at 280 nm, emission spectra were recorded from 290 to 400 nm, and the slit-widths were 4 nm.

In titration experiments, aliquots of a vesicle suspension (typically 1 mg·mL$^{-1}$) were added to the protein solution. The fluorescence intensity spectra were corrected for dilution, scatter contribution of lipid dispersions, and the inner filter effect. Absorption spectra of the samples were recorded using a Beckman DU-800 spectrophotometer. In all lipid titration experiments, the absorbance at 280 nm was less than 0.1.

To calculate the $K_d$ values, the interaction of CTC with phospholipid vesicles was treated as a 1 : 1 association. $K_d$ values were derived by nonlinear least-squares fits of data from equilibrium binding titrations of phospholipids and CTC.

To determine the binding constant between bis-ANS ($\varepsilon = 23 \times 10^3$ cm$^{-1}$ M$^{-1}$ at 395 nm) and CTC, fluorescence titration experiments were performed with 1 μM CTC in 5 mM Tris/HCl buffer (pH 7.4), incubated with 0–25 μM bis-ANS for 10 min at 25 °C. The fluorescence spectra of bis-ANS from 450 to 600 nm were obtained with excitation at 395 nm. The $K_d$ for CTC–bis-ANS complexes was calculated from the saturation curve fitted to a rectangular hyperbola. FRET from CTC Tyr residues to bound bis-ANS was performed under the same conditions. The fluorescence emission intensity was recorded from 290 to 600 nm after excitation at 280 nm. To calculate the effective energy transfer [30], CTC alone as the donor, bis-ANS alone and CTC + bis-ANS were measured.

### DSC

Calorimetry was performed in a Microcal VP differential scanning calorimeter (Microcal Inc., Northampton, MA, USA). CTC (10 μM) in 20 mM phosphate buffer (pH 7.4) was analyzed in the absence or presence of phospholipid vesicles with $T_m$ below 0 °C. All solutions were degassed just before loading into the calorimeter. Data were collected between 20 °C and 95 °C at a heating rate of 0.5 °C·min$^{-1}$. The reversibility of the thermal transition was evaluated by several cycles of heating and cooling. The standard MICROCAL ORIGIN software was used for data acquisition and analysis. The excess heat capacity functions were obtained after subtraction of the buffer baseline.

## Acknowledgements

We thank Dr G. Rivas from Centro de Investigaciones Biológicas, and G. Alvenius, Dr J. Lengqvist and Dr H. Jörnvall, Karolinska Institutet, for advice and support. This research was supported by the Swedish Research Council (project 10371), FORMAS to J. Johansson and from the Ministerio de Educación y Ciencia (SAF2006-04434), Instituto de Salud Carlos III (Ciberes-CB06/06/0002) and CAM (S-BIO-0260-2006) to C. Casals.

## References

1 Makin OS, Sikorski P & Serpell LC (2006) Diffraction to study protein and peptide assemblies. *Curr Opin Chem Biol* **10**, 417–422.
2 Westermark P (2005) Aspects on human amyloid forms and their fibril polypeptides. *FEBS J* **272**, 5942–5949.
3 Johansson J (1998) Structure and properties of surfactant protein C. *Biochim Biophys Acta* **1408**, 161–172.
4 Beers MF & Mulugeta S (2005) Surfactant protein C biosynthesis and its emerging role in conformational lung disease. *Annu Rev Physiol* **67**, 663–696.
5 Johansson J, Weaver TE & Tjernberg LO (2004) Proteolytic generation and aggregation of peptides from transmembrane regions: lung surfactant protein C and amyloid beta-peptide. *Cell Mol Life Sci* **61**, 326–335.

6 Gustafsson M, Thyberg J, Naslund J, Eliasson E & Johansson J (1999) Amyloid fibril formation by pulmonary surfactant protein C. *FEBS Lett* **464**, 138–142.
7 Nogee LM, Dunbar AE III, Wert SE, Askin F, Hamvas A & Whitsett JA (2001) A mutation in the surfactant protein C gene associated with familial interstitial lung disease. *N Engl J Med* **344**, 573–579.
8 Thomas AQ, Lane K, Phillips J III, Prince M, Markin C, Speer M, Schwartz DA, Gaddipati R, Marney A, Johnson J *et al*. (2002) Heterozygosity for a surfactant protein C gene mutation associated with usual interstitial pneumonitis and cellular nonspecific interstitial pneumonitis in one kindred. *Am J Respir Crit Care Med* **165**, 1322–1328.
9 Nogee LM (2002) Abnormal expression of surfactant protein C and lung disease. *Am J Respir Cell Mol Biol* **26**, 641–644.
10 Mulugeta S, Nguyen V, Russo SJ, Muniswamy M & Beers MF (2005) A surfactant protein C precursor protein BRICHOS domain mutation causes endoplasmic reticulum stress, proteasome dysfunction, and caspase 3 activation. *Am J Respir Cell Mol Biol* **32**, 521–530.
11 Bridges JP, Xu Y, Na CL, Wong HR & Weaver TE (2006) Adaptation and increased susceptibility to infection associated with constitutive expression of misfolded SP-C. *J Cell Biol* **172**, 395–407.
12 Sanchez-Pulido L, Devos D & Valencia A (2002) BRICHOS: a conserved domain in proteins associated with dementia, respiratory distress and cancer. *Trends Biochem Sci* **27**, 329–332.
13 Westley BR, Griffin SM & May FE (2005) Interaction between TFF1, a gastric tumor suppressor trefoil protein, and TFIZ1, a brichos domain-containing protein with homology to SP-C. *Biochemistry* **44**, 7967–7975.
14 Johansson H, Nordling K, Weaver TE & Johansson J (2006) The Brichos domain-containing C-terminal part of pro-surfactant protein C binds to an unfolded polyval transmembrane segment. *J Biol Chem* **281**, 21032–21039.
15 Hosia W, Johansson J & Griffiths WJ (2002) Hydrogen/deuterium exchange and aggregation of a polyvaline and a polyleucine alpha-helix investigated by matrix-assisted laser desorption ionization mass spectrometry. *Mol Cell Proteomics* **1**, 592–597.
16 van den Heuvel RH & Heck AJ (2004) Native protein mass spectrometry: from intact oligomers to functional machineries. *Curr Opin Chem Biol* **8**, 519–526.
17 Sobott F, Hernandez H, McCammon MG, Tito MA & Robinson CV (2002) A tandem mass spectrometer for improved transmission and analysis of large macromolecular assemblies. *Anal Chem* **74**, 1402–1407.
18 Wang WJ, Russo SJ, Mulugeta S & Beers MF (2002) Biosynthesis of surfactant protein C (SP-C). Sorting of SP-C proprotein involves homomeric association via a signal anchor domain. *J Biol Chem* **277**, 19929–19937.
19 Hyatt BA, Resnik ER, Johnson NS, Lohr JL & Cornfield DN (2007) Lung specific developmental expression of the *Xenopus laevis* surfactant protein C and B genes. *Gene Expr Patterns* **7**, 8–14.
20 Nogee LM, Dunbar AE III, Wert S, Askin F, Hamvas A & Whitsett JA (2002) Mutations in the surfactant protein C gene associated with interstitial lung disease. *Chest* **121**, 20S–21S.
21 Diakowski W & Sikorski AF (1995) Interaction of brain spectrin (fodrin) with phospholipids. *Biochemistry* **34**, 13252–13258.
22 Gazit E, Boman A, Boman HG & Shai Y (1995) Interaction of the mammalian antibacterial peptide cecropin P1 with phospholipid vesicles. *Biochemistry* **34**, 11479–11488.
23 Frey S & Tamm LK (1990) Membrane insertion and lateral diffusion of fluorescence-labelled cytochrome c oxidase subunit IV signal peptide in charged and uncharged phospholipid bilayers. *Biochem J* **272**, 713–719.
24 Schuck P & Rossmanith P (2000) Determination of the sedimentation coefficient distribution by least-squares boundary modeling. *Biopolymers* **54**, 328–341.
25 Schuck P, Perugini MA, Gonzales NR, Howlett GJ & Schubert D (2002) Size-distribution analysis of proteins by analytical ultracentrifugation: strategies and application to model systems. *Biophys J* **82**, 1096–1111.
26 Minton AP (1997) Alternative strategies for the characterization of associations in multicomponent solutions via measurement of sedimentation equilibrium. *Prog Colloid Polymer Sci* **107**, 11–19.
27 Cole JL (2004) Analysis of heterogeneous interactions. *Methods Enzymol* **384**, 212–232.
28 Laue TM, Shah BD, Ridgeway TM & Pelletier SL (1992) Interpretation of analytical sedimentation data for proteins. In *Analytical Ultracentrifugation in Biochemistry and Polymer Science* (Harding SE, Rowe AJ & Horton J, eds) pp. 99–125. Royal Society of Chemistry, Cambridge.
29 Perczel A, Park K & Fasman GD (1992) Analysis of the circular dichroism spectrum of proteins using the convex constraint algorithm: a practical guide. *Anal Biochem* **203**, 83–93.
30 Lakowicz J (1999) *Principles of Fluorescence Spectroscopy*, 2nd edn. Kluwer Academic/Plenum Publishers, New York, NY.

## Supplementary material

The following supplementary material is available online:

**Fig. S1.** Analysis of CTC disulfide bridges.

**Fig. S2.** Effects of temperature on CTC secondary structure.
**Fig. S3.** Binding of bis-ANS to CTC.

This material is available as part of the online article from http://www.blackwell-synergy.com

Please note: Blackwell Publishing are not responsible for the content or functionality of any supplementary materials supplied by the authors. Any queries (other than missing material) should be directed to the corresponding author for the article.